C. R. Mecanique 341 (2013) 211–219

Contents lists available at SciVerse ScienceDirect

Comptes Rendus Mecanique

www.sciencedirect.com

Combustion, flow and spray dynamics for aerospace propulsion

Sensitivity of swirling flows to small changes in the swirler geometry

Impact de modifications géométriques d'un swirler sur l'écoulement aval et sur le noyau tourbillonaire en précession

Jean-François Bourgouin [a,b,c,*], Jonas Moeck [a,b], Daniel Durox [a,b], Thierry Schuller [a,b], Sébastien Candel [a,b,d]

[a] *CNRS, UPR 288, laboratoire d'énergétique moléculaire et macroscopique combustion (EM2C), grande voie des vignes, 92295 Châtenay-Malabry, France*
[b] *École centrale Paris, grande voie des vignes, 92295 Châtenay-Malabry, France*
[c] *Snecma (Groupe Safran), centre de Villaroche, rond point René Ravaud-Réau, 77550 Moissy-Cramayel, France*
[d] *Institut Universitaire de France, France*

ARTICLE INFO

Article history:
Available online 11 January 2013

Keywords:
Swirling flows
Swirler design
LES
DMD
PVC

Mots-clés :
Écoulements tournants
Géométrie du swirler
SGE
DMD
NTP

ABSTRACT

Swirler design strongly influences combustion stabilization and flame dynamics in gas turbines. The rotating flow induced by the swirler is mainly determined by the swirl number. While empirical formulas may be used to estimate this quantity and deduce the corresponding flow features, a precise quantification of the impact of geometrical details is not available. This issue is investigated in this article by analyzing the sensitivity of the mean flow field and unsteady structures to small changes in the swirler design. Two radial swirlers, with slightly different geometries are compared by combining Large Eddy Simulations and experiments. The geometrical difference induces changes of the mean velocity components near the injection plane, which in turn modify the structure of the internal recirculation zone. Effects on the precessing vortex core are then revealed by applying a dynamic mode decomposition to the numerical results. It is found that the geometrical modification of the swirler notably affects the flow structure and PVC frequency.

© 2012 Académie des sciences. Published by Elsevier Masson SAS. All rights reserved.

RÉSUMÉ

La géométrie du swirler influence fortement la dynamique de flamme dans les turbines à gaz. Alors que des formules empiriques peuvent être utilisées pour estimer le nombre de swirl et l'écoulement aval correspondant, quantifier l'impact de petites modifications géométriques reste une tâche difficile. Ce problème est traité dans cet article en analysant la sensibilité de la dynamique de l'écoulement moyen et des grandes structures instationnaires à de petits changements de la géométrie du swirler. Les écoulements en aval de deux swirlers radiaux, dont la géometrie diffère légèrement, sont comparés en utilisant des simulations aux grandes échelles et des expériences. Cette différence géométrique agit fortement sur les composantes de vitesse moyenne au voisinage du plan d'injection, et sur la structure de la zone de recirculation interne. Les effets sur le noyau tourbillonaire en

* Corresponding author at: CNRS, UPR 288, laboratoire d'énergétique moléculaire et macroscopique combustion (EM2C), grande voie des vignes, 92295 Châtenay-Malabry, France.
E-mail address: jean-francois.bourgouin@ecp.fr (J.-F. Bourgouin).

1631-0721/$ – see front matter © 2012 Académie des sciences. Published by Elsevier Masson SAS. All rights reserved.
http://dx.doi.org/10.1016/j.crme.2012.10.018

précession sont ensuite étudiés à partir d'une décomposition en modes dynamiques des résultats numériques.

© 2012 Académie des sciences. Published by Elsevier Masson SAS. All rights reserved.

1. Introduction

Turbulent swirling flows are widely used in aeroengine combustors and in industrial systems like gas turbines and boilers. A high angular momentum is imposed by the swirler to the flow upstream of a sudden expansion. This generates a central recirculation zone and enhances mixing of cold fuel and oxidizer with hot gases from combustion [1] allowing stabilization of the flame at a distance from the injector surface a feature which is important for life duration and reliable combustion. However, swirling flames are sensitive to perturbations and may be subject to flashback or thermoacoustic instabilities [2]. Considerable effort is currently made to design swirlers producing compact, homogeneous and stable flames. On the downstream side of the swirler, the swirl intensity is generally characterized by the swirl number, defined as the ratio of the axial flux of azimuthal momentum to the axial flux of axial momentum (Eq. (1)):

$$S = \frac{\int_0^R \rho \bar{u}_z \bar{u}_\theta r^2 \,\mathrm{d}r}{R \int_0^R \rho \bar{u}_z^2 r \,\mathrm{d}r} \tag{1}$$

where $\bar{u}_\theta$ and $\bar{u}_z$ are the mean azimuthal and axial velocities, and pressure effects were neglected.

This number depends on the swirler geometry, and specifically on the trailing edge blades angle. Empirical relations (see for example [3]) provide estimates of the swirl number for simple designs but the flows are often assumed to closely follow the blade profile. For short blade swirlers at low Reynolds number, this assumption is often too crude and a correction is needed. This is however not straightforward. The effect of the swirl number on the downstream flow and on the flame stability is investigated in many recent studies as for example in [4] but the sensitivity of the flow to small geometrical modifications of the swirler is not well documented.

When the swirl number exceeds a critical value, a central recirculation zone is established, due to strong radial and axial pressure gradients [3]. A hydrodynamic instability of the flow in this recirculation zone and inner shear layer leads to the formation of a Precessing Vortex Core (PVC). This instability is asymmetrical and takes the shape of a simple or double helix extending along the burner axis which executes a precessing motion around this axis [5]. Studies have shown that the frequency of the PVC increases linearly with the bulk flow velocity. The variation of the dimensionless oscillation frequency, $\mathrm{S_t} = fD/u_b$ based on the frequency of the PVC f, the injector diameter D and the bulk velocity u_b, with the swirl number is not uniquely determined [5]. Analysis of the PVC is of interest because it is conjectured in some articles that it could interact with thermoacoustic instabilities [6] but the impact on the flame stability and the mechanisms of this interaction are still under discussion [7].

Swirling flows have also been extensively investigated by numerical simulations. While some Unsteady Reynolds Average Navier Stokes (RANS) simulations retrieve the PVC frequency [8], it is more appropriate to use Large Eddy Simulations (LES) to obtain further details on the flow dynamics and accurate predictions of swirling flows in cold or reactive conditions [9]. In several configurations, see for instance [10], the mean and RMS values of the unsteady velocity fields are well predicted. Unsteady phenomena, such as the PVC, can also be simulated. The PVC structure is generally identified by a pressure or vorticity isosurface in instantaneous fields [11,12]. However, a quantitative analysis is required to analyze differences between the PVC structures observed for swirlers featuring slight geometrical modifications. Pressure or vorticity contours do not allow in that case to highlight differences in a quantitative manner. A Dynamic Mode Decomposition (DMD) is employed in the present study to determine the structure of the flowfield induced by the PVC. This technique employs a large number of snapshots to retrieve a statistically meaningful representation of this unsteady flow mode. The DMD has already been successfully used to characterize various coherent structures in turbulent flows. This method has been applied for example to examine a jet in a crossflow [13].

The impact of a small geometrical modification of the swirler design on the downstream flow is analyzed in the present article using numerical simulations carried out on two similar swirlers featuring different blade lengths. One of the swirler geometries has been manufactured and tested in a combustor test rig. Predictions from LES simulations are then compared to measurements of the velocity field on the downstream side of the swirler. The structure obtained with the flow fields of the two different swirlers is discussed and a DMD is applied to the numerical results to analyze the impact on the PVC. The article begins with a brief presentation of the experimental setup.

2. Swirler designs and experimental setup

The experimental setup used in the present study (Fig. 1(a)) is similar to the one investigated by Palies et al. [14]. It is composed of a settling chamber, a nozzle, a cylindrical cavity where the radial swirler is installed, an injection tube and a transparent tube to confine the flame. Methane is mixed with air upstream the burner and the mixture is injected by two opposite pipes at the bottom of this unit. A honeycomb and a grid have been included in the plenum to break the largest

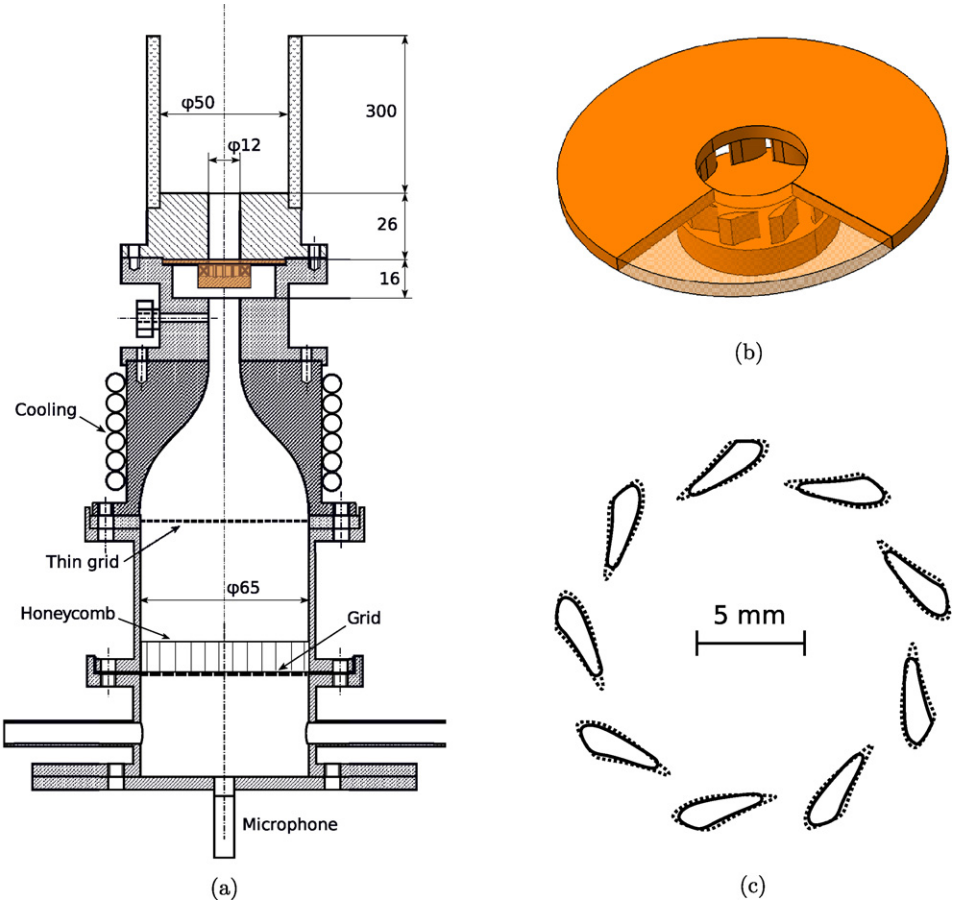

Fig. 1. (a) Schematic of the experimental setup. The swirler has been colored in orange to highlight its location in the system. All dimensions are in millimeters. (b) 3D view of the radial swirler. One quarter of the top plane has been made translucent to show the blades. (c) Comparison of two cuts of the swirlers. Dashed lines represent the original swirler design (swirler 1) and solid lines the manufactured swirler (swirler 2).

eddies and parallelize the flow. Combined with the nozzle, this enables to generate a flat profile at the swirler inlet. The combustion chamber is made of a 50 mm diameter and 300 mm long silica glass tube.

The bottom of the combustion chamber fixes the origin of the axial coordinate. The operating point is defined by a bulk flow velocity $u_b = 9.9\ \mathrm{m\,s^{-1}}$ determined in the 12 mm injection tube downstream the swirler. It corresponds to a Reynolds number, based on the injection tube diameter, $Re = 7600$ at ambient temperature. A Laser Doppler Velocimeter (LDV) enables to probe the flow in the three directions at the burner outlet. The seeded oil droplets used for LDV measurements have an average diameter of 2.5 μm enabling accurate measurements of mean and RMS velocities of the gaseous phase [15].

Fig. 1(b) shows the initial drawing of the swirler composed of nine blades, 4 mm in height. As in the experimental setup, air comes from the bottom of the swirler and is set in rotation by the blades. The diameter of the bottom plate is 20 mm while the exit diameter is 12.5 mm. This swirler has been manufactured by fast prototyping of plastic material, but due to manufacturing limitations, the fabricated piece differs from the drawing. The global shape of the blades is that of the nominal design but the blade length is shorter by about 0.8 mm. The two blade profiles are plotted in Fig. 1(c). The initial swirler is indicated by dashed lines (swirler 1) and the manufactured one appears as a continuous line (swirler 2).

3. Numerical configuration

Numerical simulations are carried out with the large eddy simulation code AVBP developed at CERFACS. This code solves the compressible Navier–Stokes equations for inert and reactive flows with unstructured meshes. In the present work, the time and space third order Taylor–Galerkin scheme [16] is used in combination with the Wale subgrid scale model.

The unstructured meshes of the swirlers, presented in Fig. 2, have been refined identically. The smallest cells (0.3 mm long) are located in the swirler, burner passage and in a frustum in the combustion chamber near the injection tube. The meshes are composed of about 6 million tetrahedra, representing about 1.1 million grid points. Only the upper part of the experimental setup, located downstream of the contraction, has been meshed. The flow can reasonably be assumed

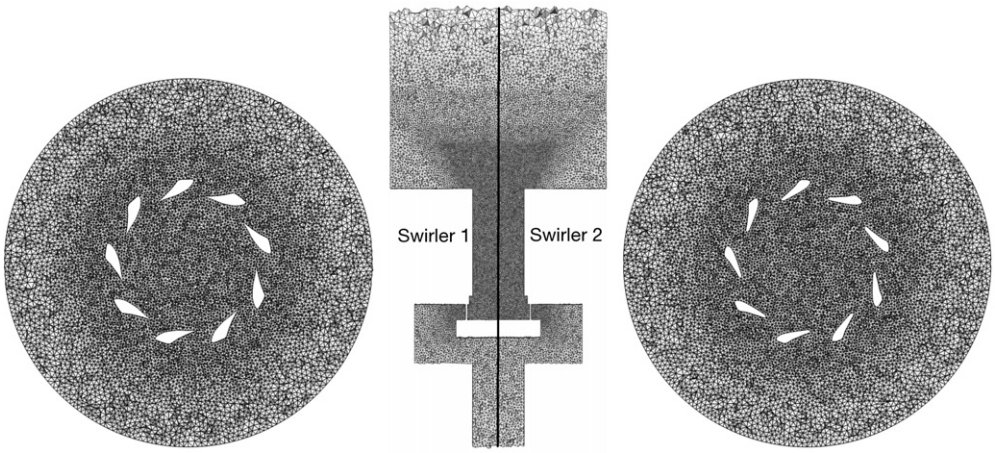

Fig. 2. Mesh resolution of the two swirler geometries.

to be laminar at the end of the contraction, so the computation of the upstream part of the plenum can be avoided. The 300 mm long quartz tube has been meshed to take into account the confinement of the downstream flow. Simulations were not run long enough to ensure convergence in the whole combustion chamber but the mean and RMS values of the velocity field did not vary after a sufficient time in the area of interest, showing that the flowfield far from the injector has a negligible impact. As it will be seen later, the internal recirculation zone is present in the entire combustion chamber. This can lead to numerical artifacts if the velocity at the outlet points towards the inside of the domain. This is avoided by making use of a cylindrical volume (1 m long and 0.8 m in diameter) added at the top of the quartz tube to ensure that large eddies are dissipated before reaching boundaries.

Boundary conditions are treated with the NSCBC formalism described in [17]. The flow inlet being considered laminar, a parabolic profile has been set to ensure adherence at the walls while conserving the total mass flow rate injected in the experiments. The experimental profile at the end of the contraction probably differs slightly from a parabola but it can be assumed that the impact is negligible for the flow downstream the swirler. The pressure has been set to 1 atm. All other boundary conditions have been treated as adiabatic and no-slip walls.

4. Results

4.1. Flowfield analysis

The mean and RMS numerical data presented in this section were obtained by averaging the unsteady velocity fields over 20 ms and over 72 vertical planes cutting the symmetry axis to obtain symmetric profiles. Experimental data were averaged over 4 s at the sampling frequency $f_e = 16$ kHz. Measurements do not always yield perfectly symmetric profiles because of uncertainties in the LDV positioning system and, to a lesser extent, because the nozzle, swirler and injection tube are not perfectly symmetric.

Fig. 3 compares the experimental mean and RMS axial velocities measured on swirler 2 and the numerical results of the two swirlers in various sections of the combustion chamber. Numerical predictions and experimental results for swirler 2 are in good agreement for the mean and RMS values. The largest difference is about 1.3 $\mathrm{m\,s^{-1}}$. At a distance $z = 2$ mm from the injection plate, the maximum velocity is 16 $\mathrm{m\,s^{-1}}$ at $r/R = 0.95$. The internal recirculation zone is present in the simulation in the entire combustion chamber. This was also observed in the experiments using smoke visualization at the tube outlet. The RMS peak is located at $r/R = 0.7$, which also corresponds to the maximum of turbulence in the inner shear layer. Fig. 4 shows that predictions for the radial mean velocities differ slightly from experimental data because in this configuration, the laser beam deviation produced by the quartz cylinder was more important introducing a bias in the measurements. The mean azimuthal velocities are also well predicted by the LES code.

The swirler geometry modification significantly influences the mean flow field and the RMS values obtained from the numerical simulations. The maximum axial and azimuthal mean velocities are higher at $z = 2$ mm for swirler 1 compared to swirler 2, respectively 5.5 $\mathrm{m\,s^{-1}}$ (32% higher for the swirler 1 compared to swirler 2) and 10.5 $\mathrm{m\,s^{-1}}$ (81% higher for the swirler 1 compared to swirler 2). At the center of the recirculation zone, the velocity is predicted with a difference of 6 $\mathrm{m\,s^{-1}}$ between the negative axial velocities. This indicates that the original swirler (swirler 1) may be more sensitive to flashback because the recirculation zone extends further upstream in the injection tube. The bulk velocity is identical for the two swirlers, but the recirculation zone is more developed for swirler 1. This emphasizes also that the swirl number is higher for swirler 1. It also features higher values for axial RMS velocities indicating that the turbulence level is higher for swirler 1. Nevertheless the peak locations are well predicted for the different axial positions z, indicating that the swirl angle is well reproduced. For all velocity components, differences between the two swirlers vanish beyond $z = 15$ mm.

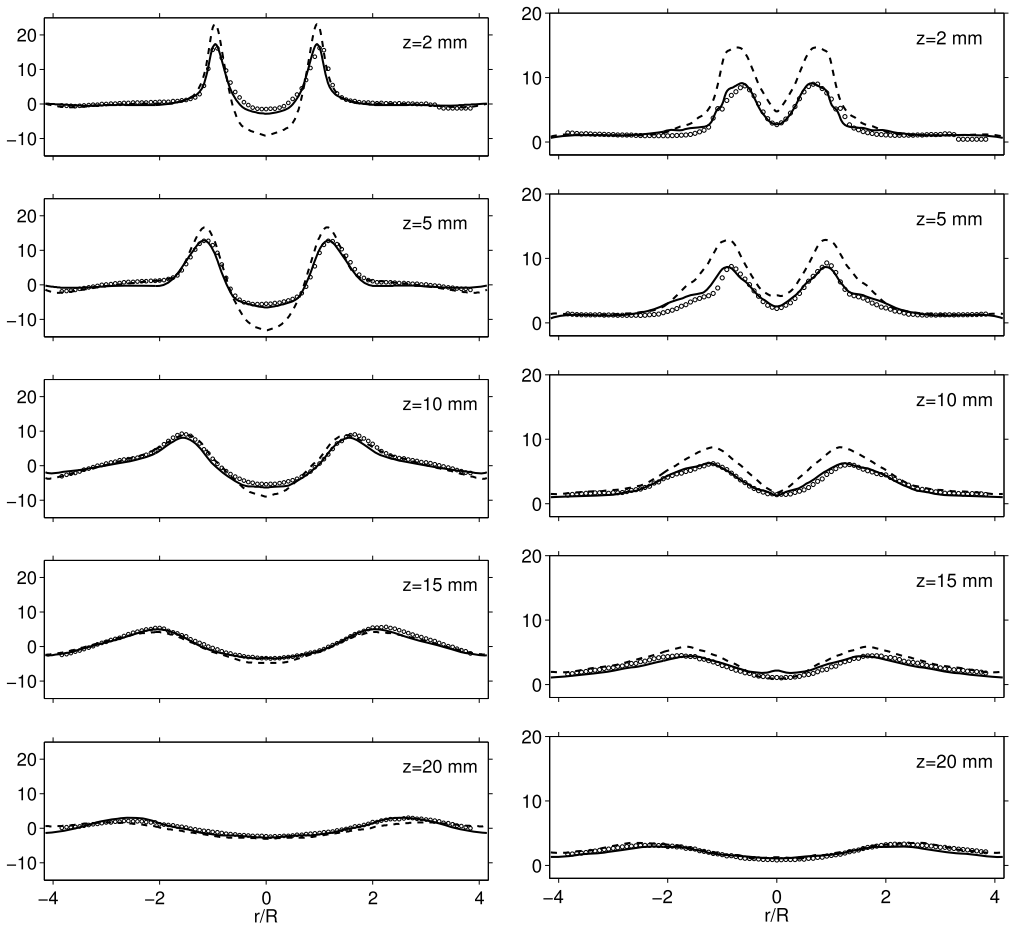

Fig. 3. Mean (left) and RMS (right) axial velocity profiles along the radial direction calculated for swirler 1 (dashed lines) and swirler 2 (solid lines) compared to experimental data (circles) at different heights z above the burner outlet. The bulk velocity for the two swirlers is $u_b = 9.88\ \mathrm{m\,s^{-1}}$.

Fig. 5 shows the velocity vectors in a horizontal plane colored by the modulus of the velocity for the two geometries investigated. This figure highlights that small differences of swirler geometry induce strong changes in the flowfield. In particular, the flow deviation in the azimuthal direction is stronger for swirler 1. The area blockage is also higher, due to longer blades resulting in an acceleration of the flow inside the swirler. For swirler 2, velocities are smaller and streamlines do not follow the blade profiles. Flow separation appears near the leading edge of the blade. This explains why the swirl number induced by swirler 1 is stronger than that of swirler 2. These two swirl numbers can be calculated using the azimuthal and axial mean velocity profiles at the burner outlet using Eq. (1). One finds 0.84 for swirler 1 and 0.70 for swirler 2.

4.2. Dynamic mode decomposition study of the PVC

Dynamic Mode Decomposition (DMD) can now be used to extract the essential dynamical features from large space–time datasets [13,18]. Consider a set of data composed of n samples acquired at regular time intervals Δt. Each sample contains m data corresponding to one physical quantity. For instance, m can be the number of unknowns in the area of interest. Typical orders of magnitude for datasets issued from numerical simulations are $n \sim 10^2$ and $m \sim 10^6$. One defines v_i the vector representing the data sampled at time $t_i = i\Delta t$ and V_i^j the matrix of the data acquired from time $t_i = i\Delta t$ to $t_j = j\Delta t$:

$$V_i^j = \{v_i, v_{i+1}, \ldots, v_j\} \tag{2}$$

It is now assumed that the dynamics of the system, represented by the data set, is governed by a linear operator A that maps the system state at time step $n-1$ to that at time step n: $AV_1^{n-1} = V_2^n$. In this case, the complex eigenvalues of A represent the characteristic frequencies and the growth rates of particular oscillation modes. However, the size of A is $m \times m$ and the manipulation of this matrix requires large computational resources. The objective is then to define a matrix S which is of companion type and has similar eigenmodes and eigenvalues as A [19] by setting:

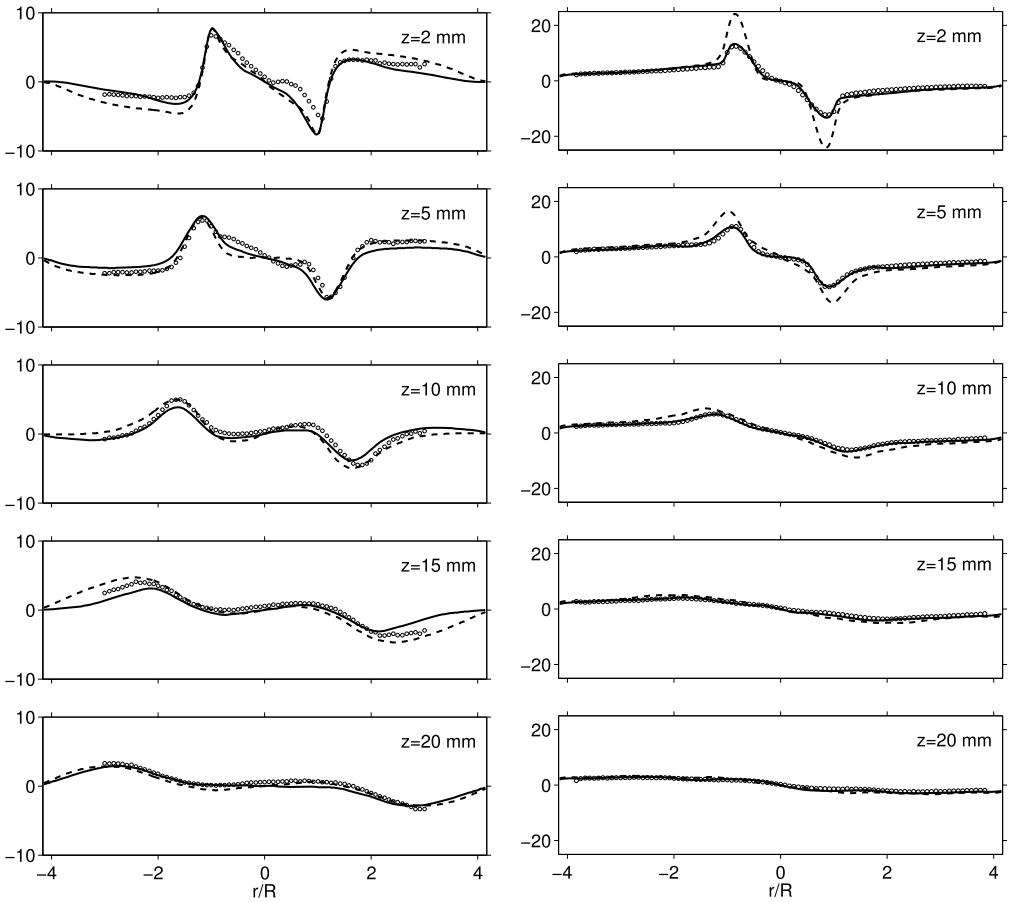

Fig. 4. Mean radial (left) and azimuthal (right) velocity components along the radial direction calculated for swirler 1 (dashed lines) and swirler 2 (solid lines) compared to experimental data (circles) at different heights z above the burner outlet. The bulk velocity for the two swirlers is $u_b = 9.88\ \mathrm{m\,s^{-1}}$.

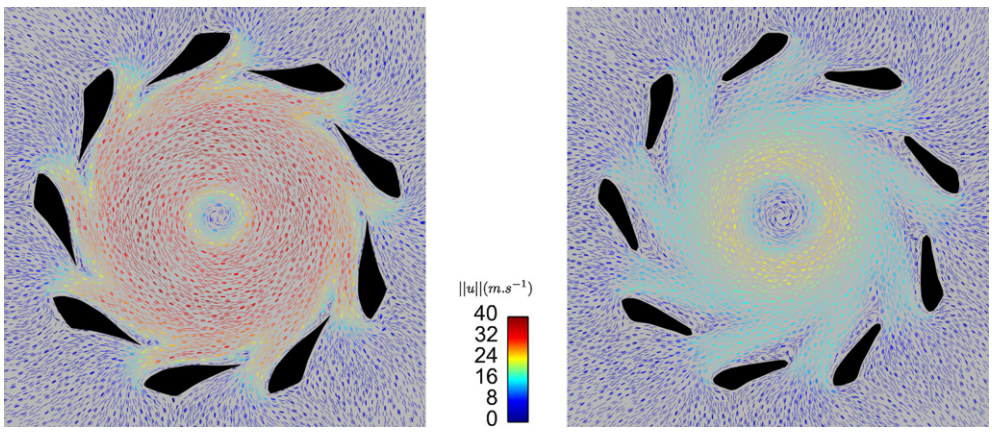

Fig. 5. Velocity field, colored by the velocity magnitude, in a section at the middle of the swirler height (2 mm) for swirler 1 (left) and swirler 2 (right).

$$S = \arg\min_{M} \left\| V_2^n - V_1^{n-1} M \right\| \tag{3}$$

where S is a relatively small $(n-1)\times(n-1)$ matrix that can be diagonalized. One also defines λ_j the eigenvalues of S and X_j the corresponding matrix of eigenvectors. The jth dynamic mode DM_j is obtained by projecting the jth eigenvector onto the snapshot basis: $DM_j = V_1^n X_j$. The frequencies $f_j = \omega_j^{freq}/2\pi$ and the growth rates ω_j^{grow} can also be retrieved by using the complex eigenfrequency $\omega_j = \omega_j^{grow} + i\omega_j^{freq}$ which verifies $\lambda_j = \mathrm{e}^{\omega_j \Delta t}$.

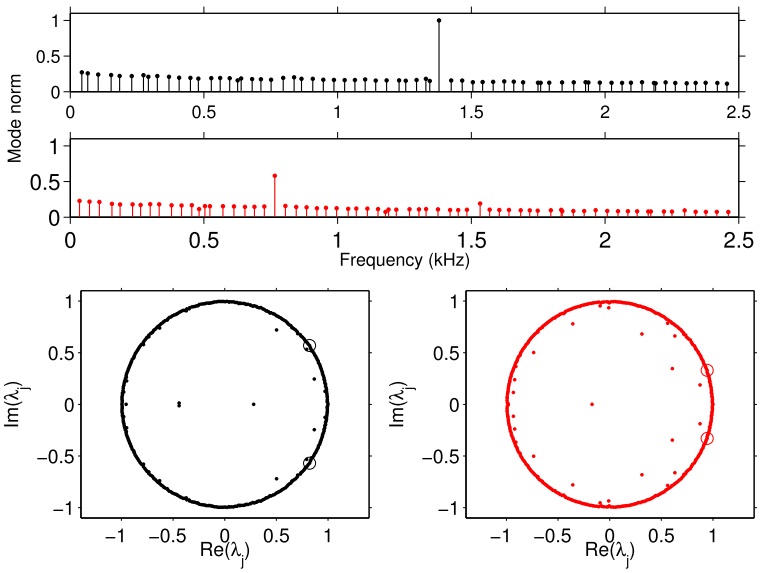

Fig. 6. DMD spectrum (top) of axial velocity for swirler 1 (black) and swirler 2 (red) for a bulk flow velocity of 9.88 $\mathrm{m\,s^{-1}}$ calculated on 390 3D instantaneous solutions at a sampling frequency $f_s = 14$ kHz. Plot of the complex eigenvalues for swirler 1 (bottom left) and swirler 2 (bottom right). The open circles correspond to the modes at 1378 Hz for swirler 1 and 682 Hz for swirler 2.

To analyze the PVC structure with this technique, one would have to apply the DMD to the three velocity components. One possibility is to include all the components in the vectors v_i. It was found however that it was sufficient to calculate the DMD from a single velocity component. The remaining two components were constructed by projecting the eigenvectors X_j onto the snapshot basis corresponding to these components. In the following, u, v and w represent the three velocity components in a cartesian frame of reference, and respective superscripts are used to indicate that eigenvectors and dynamic modes have been calculated on the basis of the dataset for this velocity component. For instance, S^u is the companion matrix which has been calculated with the u velocity component. When this matrix is diagonalized one obtains the eigenvalues λ_j^u and the correspondent eigenvectors X_j^u. The modes are calculated for the three components by using only the eigenvectors obtained for the velocity component u such as: $DM_j^u = V_1^{u,n-1} X_j^u$, $DM_j^v = V_1^{v,n-1} X_j^u$ and $DM_j^w = V_1^{w,n-1} X_j^u$. This approach is admissible because the PVC represents a globally synchronized oscillation in which all three velocity components participate.

The DMD modes have to be scaled by an appropriate norm. To recover the values in meters per second, the modes can be divided by the scaling factor $S_f = \sum_i X_m(i)$ where X_m is the DMD mode which corresponds to the eigenvalue $\omega_m = 0$.

The proposed technique is applied to 390 instantaneous 3D solutions sampled at a frequency $f_s = 14$ kHz. Fig. 6 shows the modulus of the DMD modes as a function of frequency. One can see that the PVC frequency emerges at 1378 Hz for swirler 1 and at 765 Hz for swirler 2. For swirler 2, the frequency measured in experiments for the PVC is 682 Hz which differs by less than 12% from the computed one. It is interesting to note that the PVC frequency is sensitive to the swirl number. A variation of 20% of the swirl number yields a change of 80% in the PVC frequency because the PVC depends on the maximum azimuthal component which has increased by 81%. No other periodic phenomena are visible.

Fig. 7 shows the streamlines obtained with the DMD calculated on the axial component of the velocity 2 mm above the inlet plane of the combustion chamber. The figure is colored by the axial velocity obtained by DMD, and the region of reverse flow is indicated by a white contour. These figures are qualitatively similar for the two swirlers. The vortex core lies at the boundary of the reverse-flow region and precedes the zone of negative axial velocities in the rotation cycle. This is consistent with experimental and numerical results from other studies on PVC dynamics, for example [20,21]. The maximum axial velocity lies near the vortex core, indicating that this structure accelerates the flow. The modification of the swirler design also has an impact on the PVC shape. The velocities are higher and the recirculation zone is wider for swirler 1, which is coherent with the mean axial velocity profiles shown in Fig. 3. The complex discrete-time eigenvalues λ_j plotted in Fig. 6 indicates that modes are, in this case, mainly located on the unit circle. It can be infered that the PVC has reached its maximum amplitude and that any transient solution components associated with the initial conditions have vanished.

To study the difference of PVC structures induced by the two swirlers, an axial slice of the axial velocity mode obtained by DMD at the PVC frequency is plotted in Fig. 8. The shape of the PVC is qualitatively similar near the injection tube exit, explaining why the two streamline plots also feature similar patterns as observed in Fig. 7. One finds that the PVC amplitude is higher for swirler 1 and that the shape of the PVC is qualitatively different. For swirler 2, the general form is that of a helix and the PVC vanishes after one injection tube diameter. For swirler 1, the situation is different. There is no

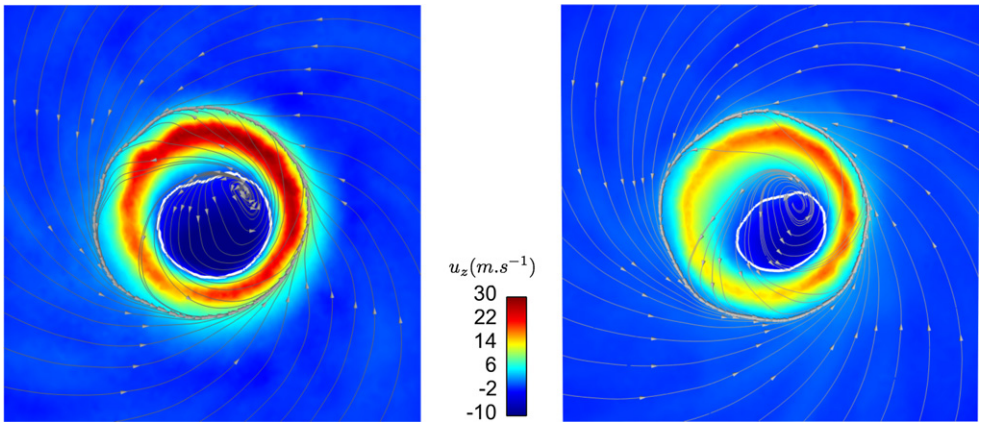

Fig. 7. Pseudo-streamlines obtained with the radial and azimuthal components of the velocity of the DMD mode of the PVC, at 2 mm above the inlet plane of the combustion chamber for swirler 1 (left) and swirler 2 (right). The field is colored by the axial velocity. The region of reverse flow is indicated by the white contour.

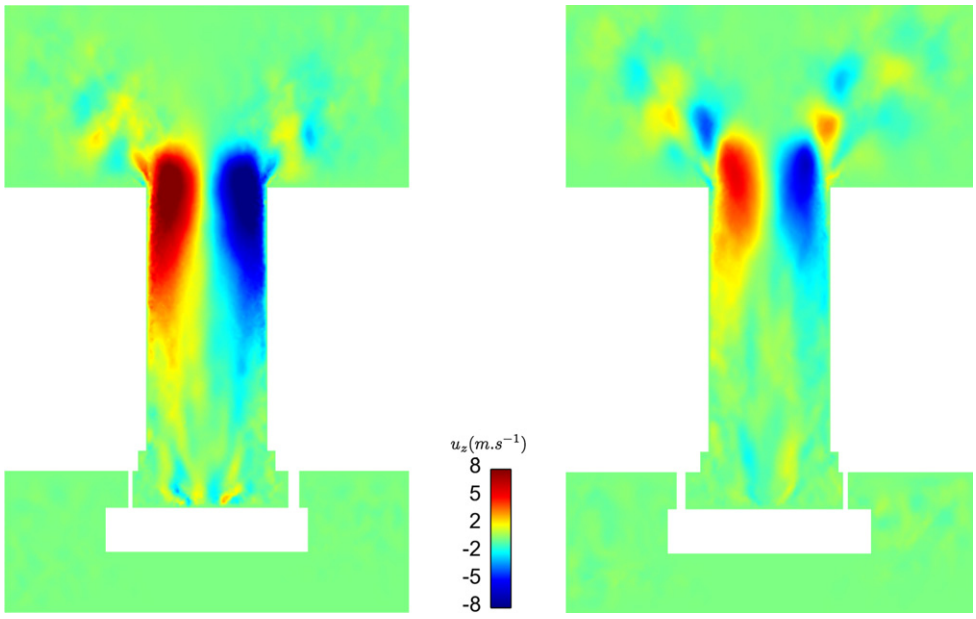

Fig. 8. Longitudinal cut of axial velocity of the first DMD mode. Left: swirler 1 at $f_{PVC} = 765$ Hz; Right: swirler 2 at $f_{PVC} = 1378$ Hz.

distinct pattern in the combustion chamber because the PVC amplitude decreases rapidly after one third of the injection tube diameter.

5. Conclusion

The impact of a small modification of the swirler geometry on the downstream flow is investigated in this article by considering two swirlers with slightly different geometries. Large eddy simulations have been carried out in the two cases. One of them has been manufactured and tested in a test rig combustor configuration. Experimental data are in good agreement with computations for axial and azimuthal mean velocities and for axial RMS velocities in different axial sections of the system. The swirler modification which consists in an increase in the blade length by 0.8 mm (20% of the initial blade length), augments the maximum axial and azimuthal mean velocities by a factor of respectively 32% and 81% at 2 mm downstream of the combustor back plane and leads to an increase in the RMS velocity levels and in the swirl number. A dynamic mode decomposition has been applied to the LES numerical results to analyze the unsteady behavior. This is used to identify a strong periodic component with low level harmonics characteristic of the PVC. This structure lies close to the boundary of the reverse-flow zone and precedes this region in the rotation cycle. The swirler design notably influences the PVC. With an increase in the swirl number, the internal recirculation zone expands in the transverse direction. The frequency is also increased by 80% which corresponds to the local rise of the mean azimuthal velocity. Moreover the amplitude of the PVC is

larger but vanishes at a lower height in the combustion chamber. The shape of the helical perturbation is also less apparent for an increased value of the swirl number.

Acknowledgements

This work has been supported by the Agence nationale de la recherche, contract No. ANR-08-BLAN-0027-01, DGA (Délégation générale pour l'armement), and by Snecma (Safran Group). This work was granted access to the HPC resources of CINES under the allocation 2011-020164 made available by GENCI (Grand Equipement National de Calcul Intensif). The authors wish to thank J. Beaunier, E. Jean-Bart and Y. Le Teno for the technical support provided to this research.

References

[1] O. Lucca-Negro, T. O'Doherty, Vortex breakdown: A review, Progress in Energy and Combustion Science 27 (4) (2001) 431–481.
[2] S. Candel, Combustion dynamics and control: Progress and challenges, Proceedings of the Combustion Institute 29 (1) (2002) 1–28.
[3] A.K. Gupta, D.G. Lilley, N. Syred, Swirl Flows, Abaqus Press, 1984.
[4] C. Hirsch, D. Fanaca, P. Reddy, W. Polifke, T. Sattelmayer, Influence of the swirler design on the flame transfer function of premixed flames, in: Proceedings of the ASME Turbo Expo 2005, vol. 2, 2005, pp. 151–160.
[5] N. Syred, A review of oscillation mechanisms and the role of the precessing vortex core (PVC) in swirl combustion systems, Progress in Energy and Combustion Science 32 (2) (2006) 93–161.
[6] A.M. Steinberg, I. Boxx, M. Stöhr, C.D. Carter, W. Meier, Flow-flame interactions causing acoustically coupled heat release fluctuations in a thermo-acoustically unstable gas turbine model combustor, Combustion and Flame 157 (2010) 2250–2266.
[7] J.P. Moeck, J.F. Bourgouin, D. Durox, T. Schuller, S. Candel, Nonlinear interaction between a precessing vortex core and acoustic oscillations in a turbulent swirling flame, Combustion and Flame 159 (8) (2012) 2650–2668.
[8] B. Guo, T.A.G. Langrish, D.F. Fletcher, CFD simulation of precession in sudden pipe expansion flows with low inlet swirl, Applied Mathematical Modelling 26 (2002) 1–15.
[9] A. Sengissen, J. Vankampen, R. Huls, G. Stoffels, J. Kok, T. Poinsot, LES and experimental studies of cold and reacting flow in a swirled partially premixed burner with and without fuel modulation, Combustion and Flame 150 (1–2) (2007) 40–53.
[10] P. Wang, X.S. Bai, M. Wessman, J. Klingmann, Large eddy simulation and experimental studies of a confined turbulent swirling flow, Physics of Fluids 16 (9) (2004) 3306–3324.
[11] S. Roux, G. Lartigue, T. Poinsot, U. Meier, C. Bérat, Studies of mean and unsteady flow in a swirled combustor using experiments, acoustic analysis, and large eddy simulations, Combustion and Flame 141 (1–2) (2005) 40–54.
[12] Y. Huang, V. Yang, Dynamics and stability of lean-premixed swirl-stabilized combustion, Progress in Energy and Combustion Science 35 (4) (2009) 293–364.
[13] C.W. Rowley, I. Mezić, S. Bagheri, P. Schlatter, D.S. Henningson, Spectral analysis of nonlinear flows, Journal of Fluid Mechanics 641 (2009) 115–127.
[14] P. Palies, D. Durox, T. Schuller, P. Morenton, S. Candel, Dynamics of premixed confined swirling flames, C. R. Mécanique 337 (6–7) (2009) 395–405.
[15] D. Durox, S. Ducruix, F. Lacas, Flow seeding with an air nebulizer, Experiments in Fluids 27 (1999) 408–413.
[16] O. Colin, M. Rudgyard, Development of high-order Taylor–Galerkin schemes for LES, Journal of Computational Physics 162 (2) (2000) 338–371.
[17] T.J. Poinsot, S.K. Lele, Boundary-conditions for direct simulations of compressible viscous flows, Journal of Computational Physics 101 (1) (1992) 104–129.
[18] P.J. Schmid, L. Li, M.P. Juniper, O. Pust, Applications of the dynamic mode decomposition, Theoretical and Computational Fluid Dynamics 25 (1–4) (2010) 249–259.
[19] P.J. Schmid, Dynamic mode decomposition of numerical and experimental data, Journal of Fluid Mechanics 656 (2010) 5–28.
[20] M. Garcìa-Villalba, J. Fröhlich, W. Rodi, Numerical simulations of isothermal flow in a swirl burner, Journal of Engineering for Gas Turbines and Power 129 (2007) 377–386.
[21] P.M. Anacleto, E.C. Fernandes, M.V. Heitor, S.I. Shtork, Swirl flow structure and flame characteristics in a model lean premixed combustor, Combustion Science and Technology 175 (8) (2007) 1369–1388.